

Research article

MSPA-based green space morphological pattern and its spatiotemporal influence on land surface temperature

Ming Chen^a, Yubo Sun^b, Bo Yang^c, Jiayi Jiang^{d,e,*}

^a College of Landscape Architecture and Art, Fujian Agriculture and Forestry University, Fuzhou, 350100, People's Republic of China

^b School of Software and Microelectronics, Peking University, Beijing, 100871, People's Republic of China

^c School of Landscape Architecture and Planning, The University of Arizona, Tucson, AZ, 85719-0075, USA

^d Department of Landscape Architecture, School of Architecture, Soochow University, No. 199 Ren-ai Road, Suzhou Industrial Park, Suzhou, 215123, People's Republic of China

^e China-Portugal Joint Laboratory of Cultural Heritage Conservation Science Supported by the Belt and Road Initiative, Suzhou, 215123, People's Republic of China

ARTICLE INFO

Keywords:

Urban thermal environment
Spatial pattern
Spatiotemporal regression analysis
Spatiotemporal non-stationarity

ABSTRACT

The frequent occurrence of extreme heat events has notably affected human's living environment, and a considerable number of studies have reported that green space is an efficient measure by investigating the correlation between green space and land surface temperature (LST). However, spatiotemporal effects of green space on LST still remain unclear. In this study, green space patterns (e.g., core, islet, perforation, edge, loop, bridge, and branch) were identified through morphological spatial pattern analysis (MSPA). Moreover, the effects of green space pattern on LST in three periods were investigated through three kinds of models. As indicated by the results: (1) the geographically and temporally weighted regression model exhibited the optimal performance compared with other two models. (2) in general, the core, the edge, the bridge, and the branch significantly contributed to cooling, and the islet hindered cooling. However, the perforation and the loop exerted significant dual nature effects with the similar quantity of the negative and positive coefficients, showing relatively complex impact mechanism. (3) the intensity of the effect of the respective MSPA class varied across the study area. The core had the most substantial effect, which distributed in the south and middle corners. (4) the result suggested that a neighborhood scale in China, which was 960 m in this study, served as a basic unit in green space management. The spatiotemporal non-stationarity of the effects of green space morphological patterns on LST provided important insights into urban thermal environment improvement through urban green space planning and design.

1. Introduction

Extreme heat events occurred more and more frequently in recent years, which has notably affected human's daily life. It is noteworthy that an increasingly higher land surface temperature (LST) results in a wide variety of problems (e.g., air pollution,

* Corresponding author. Department of Landscape Architecture, School of Architecture, Soochow University, No. 199 Ren-ai Road, Suzhou Industrial Park, Suzhou, Jiangsu Province, People's Republic of China.

E-mail addresses: hustchenming@163.com (M. Chen), syb2000417@stu.pku.edu.cn (Y. Sun), boyang17@email.arizona.edu (B. Yang), jjjiang@suda.edu.cn (J. Jiang).

<https://doi.org/10.1016/j.heliyon.2024.e31363>

Received 13 July 2023; Received in revised form 12 May 2024; Accepted 15 May 2024

Available online 18 May 2024

2405-8440/© 2024 The Authors. Published by Elsevier Ltd. This is an open access article under the CC BY-NC license (<http://creativecommons.org/licenses/by-nc/4.0/>).

decreased energy efficiency, thermal discomfort, and harmful health effects) [1–4]. Notably, urban green space is capable of efficiently alleviating LST, mainly due to the effect of evapotranspiration and shading of vegetation [5–8]. In general, green space comprises any vegetation area in the urban environment [9]. To be specific, at a micro level, various green space areas, perimeters, patterns, and tree species, vegetation configuration, planting design, and facade greening can result in the generation of different cooling effects and thermal comfort [10–15]. The local air or surface temperature can be even reduced by pocket parks, green roofs, and street trees in a high-density area [16–18]. Besides, at a macro level, a change in the green space system significantly affects the spatial pattern of the urban thermal environment [19,20]. To guide green space practice, Zhang et al. [21] found that area metrics of green spaces play an important role in predicting local surface temperatures. Kubota et al. [22] have developed several green space planning strategies to obtain differences in their cooling effects through simulation. The expansion of urban green space areas can lead to directly and effectively reduced LST, whereas its method does not practically apply to most cities. Accordingly, a proper arrangement and spatial pattern of green space should be considered to form a better spatial pattern of an urban thermal environment.

The effect of green space spatial pattern on LST has been investigated in extensive research, where the spatial pattern of the green space was primarily measured with the landscape composition and configuration metrics that included the size, density, edge, shape, and connectivity of green space [21,23–26]. Most studies have suggested that the green space with a larger scale tends to exhibit a lower LST, primarily manifested as a significantly negative correlation among the percentage of landscape (PLAND), mean patch area (AREA_MN), largest patch index (LPI) and LST [21,27–31]. In addition, a positive correlation was usually found between LST and the mean fragmentation index (FD), Euclidian nearest neighbor distance (ENN_MN), patch cohesion index (COHESION), suggesting that a higher connectivity is conducive to exhibit a lower LST [24,32,33]. However, the correlation between some metrics and LST exhibits conflicting results. For instance, the effects of patch density (PD) and landscape shape index (LSI) on LST varied among study sites [31, 34]. Pramanik and Punia [31] suggested that green space with a regular and straightforward shape was conducive to reduce LST, whereas Jia and Zhao [23] suggested an irregular green space shape. The edge density (ED) was negatively correlated with LST [30, 35], whereas a positive correlation was found in other studies [29,36]. In addition, the above-mentioned landscape metrics focus on the composition and configuration of green space and reflect quantitative values of green space spatial patterns, making it challenging to take adequate measures for LST mitigation.

Complex impact mechanisms of green space on LST have attracted many scholars to conduct research from various aspects. With the rapid urbanization and the removal of green spaces, fragmentation and isolation in the green spaces increased significantly, which reduced the potentiality of green space as a cooling mechanism over the city [37]. As an important component of green space, city parks are usually considered as a key element for LST mitigation [38]. The relative contribution of composition and configuration of green space patterns to LST was identified in an urban agglomeration study, where the magnitude of contribution of different green space patterns varied [39]. Moreover, other studies indirectly concluded the influence of green space on LST. For example, Das et al. found that the relationship between the quality of living and green space was negative, which may promote several environmental problems, such as the emergence of the UHI effect [40].

On that basis, the correlation between green space and LST should be explored using a quantitative metric that can characterize green spaces in a spatially explicit way. Thus, the green space morphological pattern can be evaluated through morphological spatial pattern analysis (MSPA), i.e., an image-processing method that has been preliminarily adopted to study the simple linear correlation between green space and LST based on several sample sites [41]. MSPA has been recently adopted to examine spatiotemporal dynamics of urban green space [42]. It was also used to identify heat sources [43,44]. Furthermore, MSPA was combined with other methods to make a deeper study, especially for network construction. Luo et al. [45] applied MSPA and landscape connectivity indexes to identify heat island and cold island patches. Zhao et al. [46] adopted circuit theory to identify the thermal connectivity corridors and key nodes among heat island sources based on MSPA. Jiang et al. [47] constructed a heat exposure spreading network and a green infrastructure network using MSPA and circuit theory, so as to propose key areas and measures to mitigate heat exposure risk. Liu et al. [48] integrated the above methods to construct a cold island network for the urban heat island effect mitigation. Other methods, including two-step floating catchment area, minimum cumulative resistance model, were also applied in research on thermal environments and green space [49,50]. In addition, the non-linear correlation has been found between green space pattern and urban heat island intensity at a 3-km grid size [51]. As the important components of green space, grassland, wetland, and forest were taken as research objects in different studies, usually used for cold island patches identification [52–54].

Most relevant research has considered the effect of green space spatial pattern on LST to be spatially stationary and used a global regression, mainly for ordinary least squares (OLS), or the Pearson correlation to analyze their correlation [29,35,55–57]. However, there are significant differences in LST across urban areas that have numerous influences. The above-described methods also ignored spatial non-stationarity and the spatial dependence of variables [58]. Other studies have used spatial regression models (e.g., spatial lag model, spatial error model, and general spatial model) to optimize the regression results [59,60]. A local regression (e.g., geographically weighted regression (GWR)) was also employed for analysis between LST and land cover, urban morphology, or landscape characteristics [61–63], whereas it has been rarely employed for green space pattern analysis, especially MSPA method. Basu et al. [64] used GWR, multiscale GWR, and robust GWR to explore correlation between green space landscape pattern and LST. However, temporal effect of green space on LST was not included in their study. Besides, results of these methods usually focus on the spatial distribution of each independent variable. However, the quantity of regression coefficient, which reflects the influence strength of independent variables on the dependent variable, has rarely been considered. Since LST and green space are dynamic, this issue should be considered in the study of green space and LST.

Overall, there are two gaps in the knowledge regarding the green space spatial patterns and LST. Firstly, although MSPA was widely used in the LST and green space studies, this method was usually used for cold or hot island identification or network construction. There is rare research on quantitatively revealing the relationship between green space morphology and LST, especially in further

revealing the spatial differences in the impact of green space on LST. Secondly, spatiotemporal effects of green space on LST still remain unclear. Although most previous studies on the green spaces and LST have considered multiple periods, they have mostly compared the impacts of green space on LST in different periods [24,64,65]. In this way, the temporal characteristics of green space and LST cannot be reflected. The spatiotemporal influence mechanism needs to be paid more attention to provide reference for the green space optimization.

Based on the above-mentioned limitations, this study was conducted to investigate the spatiotemporal non-stationarity of the effects of green space morphological patterns on LST. This study aimed to: (1) examine the spatiotemporal pattern of green space morphological pattern characterized by MSPA, LST, and its spatial auto-correlation, (2) assess the spatiotemporal non-stationarity of the effect of green space morphological patterns on LST using geographically and temporally weighted regression (GTWR), and (3) investigate the spatial sensitivity of the above correlations to determine an optimal scale for practice.

2. Data and methods

2.1. Study site

Wuhan (113°41′-115°05′ E, 29°58′-31°22′ N), the capital of the Hubei Province, is a megacity and is known as one of the “four ovens” in China. It has a subtropical monsoon climate with an annual mean temperature of 17 °C in recent years.

The downtown area of Wuhan was divided into three areas, Hankou, Hanyang, and Wuchang, by the Yangtze River and the Hanjiang River (Fig. 1). Since LST is affected by a wide variety of factors and that the study area should be representative, Hankou was selected for analysis for the following reasons: (1) Hankou has a higher population density compared with the other two areas, where people may be in a worse environment with higher LST (2) the area of the water body (e.g., rivers and lakes) is the least in Hankou, reducing the interference of water bodies on LST regulation; (3) diversified green spaces are densely distributed in Hankou (e.g., park green space, attached green spaces, and ecological green spaces). The spatial distribution of the above-described green spaces reflects

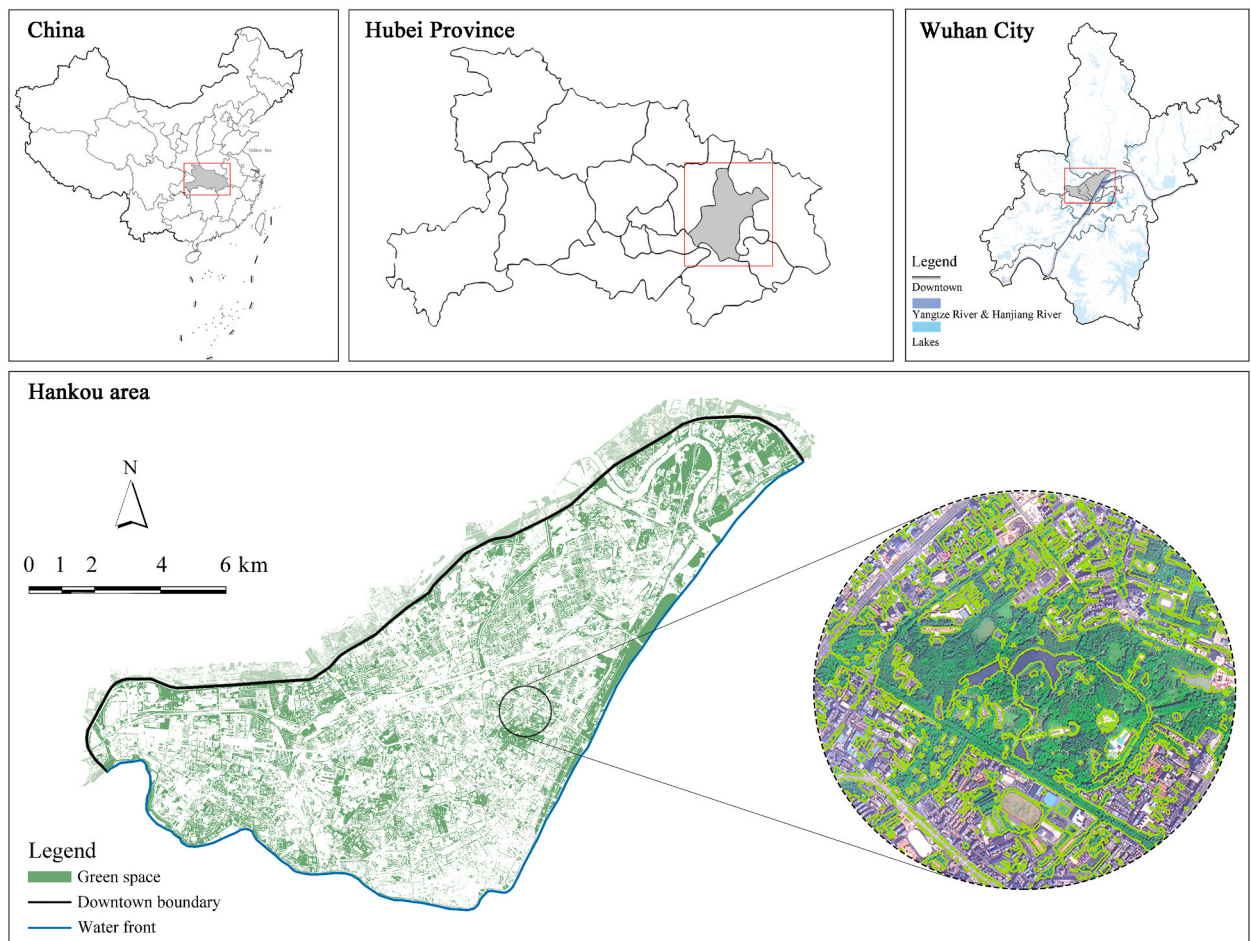


Fig. 1. Location and green space distribution of the study site. (For interpretation of the references to color in this figure legend, the reader is referred to the Web version of this article.)

the typical characteristics of megacities (Fig. 1). In brief, the study site was an integral land that did not contain large water bodies, with an area of nearly 138 km².

2.2. Research methods

A methodological framework was built to analyze the spatiotemporal effect of green space morphological pattern on LST (Fig. 2). First, the green space vector data were obtained from Gaofen-2 imageries and Google earth imageries to calculate seven MSPA classes indicators, and LST was retrieved from Landsat-7 and Landsat-8 imageries. Second, four scales were determined to evaluate the optional scale on LST study. Then, multicollinearity test and auto-correlation analysis were conducted before regression model construction to ensure rationality of the regression model to be built. Furthermore, the correlation between MSPA classes and LST was examined through OLS, GWR, and GTWR models. Although these methods are commonly used, GTWR is rarely applied in the studies on green space and thermal environment, thereby revealing spatiotemporal influence of green space on LST. Notably, the statistics of regression coefficient was used to reveal the spatiotemporal non-stationarity of the influence pattern and strength of MSPA classes on LST. Finally, implications for green space planning and design were put forward according to the above quantitative analysis.

2.3. Data source and pre-processing

Three periods indicating the early, middle and late stages of rapid urbanization (2006, 2013, and 2017/2018) were selected to represent the development of green space and LST. Firstly, the green space was extracted using high-resolution remote sensing imageries with a 0.8-m spatial resolution taken by Gaofen-2 satellite in 2016 as the basis for obtaining green space data for three periods. Then, green space data in 2006, 2013 and 2017 were adjusted based on the data acquired in 2016 through Google earth history imageries (0.26-m spatial resolution). LST was retrieved in different years using Landsat-7 and Landsat-8 imageries with a 30-m spatial resolution. In general, the acquired data achieved the cloud cover of less than 10 %, and no cloud cover was observed in the study area. Table 1 lists the detailed information of the above-mentioned remote sensing imageries of the three years. The data of adjacent periods were selected for analysis. Due to the accessibility of Google earth history imageries in 2006, the winter season was considered for analysis. We can still accurately identify green space area through the morphology and texture of trees by means of the high resolution of Google earth imageries. Even though the last period spanned over one year, green spaces were nearly unchanged from 2017 to 2018 in the study area, such that they are considered appropriately comparable. Two types of imageries were first radiometrically calibrated prior to green space extraction and LST retrieval. Since Landsat-7 was subjected to the stripe loss problem, strip repairing was conducted using ENVI plug-in components. Subsequently, the imageries for green space extraction were rectified and georeferenced to the Landsat imageries. Furthermore, the FLAASH atmospheric correction was performed for the above-described data.

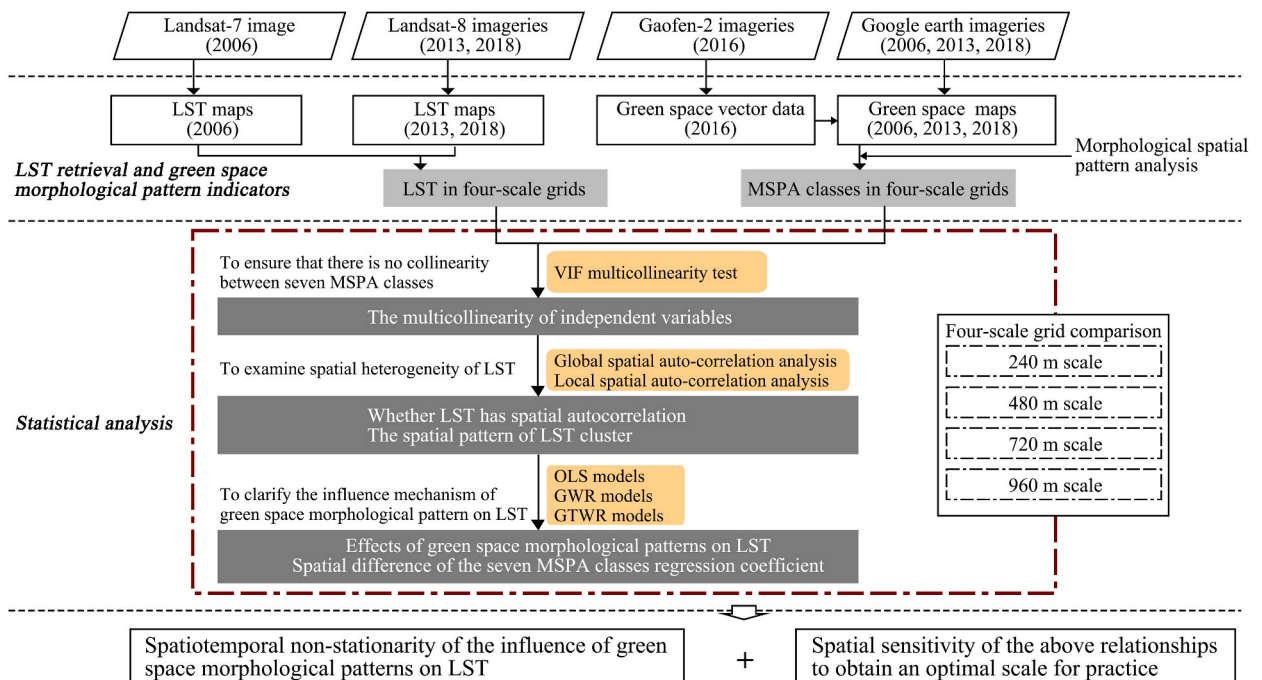


Fig. 2. Methodology flowchart used in this study.

Table 1
Attributes of the remote sensing imageries.

Imageries for green space extraction				Imageries for LST retrieval			
Satellites	Sensors and bands	Cloud cover in study area	Acquisition dates	Satellites	Sensors and bands	Cloud cover in study area	Acquisition dates
Gaofen-2	PMS 3 and 4	0	2016-09-01	Landsat-7	ETM+ 6	0	2006-07-18
Google earth	/	0	2006-12	Landsat-8	TIRS 10	0	2013-07-31
	/	0	2013-07	Landsat-8	TIRS 10	0	2018-09-15
	/	0	2017-07				
	/	0					

Note: Acquisition dates of Google Earth cannot be precise to the day.

2.3.1. Green spaces extraction and morphological patterns calculation

The accurate green space maps were obtained using three high-resolution imageries. The object-oriented classification method was performed to accurately extract green space using ENVI 5.4 software on the patch level [66]. Normalized difference vegetation index (NDVI) has been confirmed as a vital index to identify green space; it was determined based on the near-infrared band and the red band [67,68]. Subsequently, the vector data of the green spaces were extracted based on a certain threshold of NDVI. In this study, green space was more effectively identified under the NDVI of a pixel of over 0.7. Next, visual interpretation was performed to optimize the results using the ArcGIS 10.7 software, such that green spaces can be mapped with the maximum accuracy (Fig. 1). On that basis, green space vector data in 2006, 2013, and 2017 were adjusted manually according to Google Earth history imageries in the three years.

MSPA involves a number of image processing techniques that can identify and measure raster data at the pixel level based on mathematical morphological techniques such as erosion, dilation, opening, and closing operations [69]. Given the above data, green space was considered foreground and others was regarded as background. They were converted into the binary raster data in a TIFF format. Subsequently, the data were inputted into Guidos Toolbox software for morphological spatial pattern analysis. The core is identified first based on the connectivity rule (four or eight neighbors) and edge width value. With the increase in edge width, the minimal size of core increases and the number of pixels classified as core reduces, which results in gains for other MSPA classes. For example, with the increase in edge width, a linear small-area core can be changed to bridge or branch. Due to edge effect, two parameters—the spatial resolution of the input binary raster data and the size parameter set in the software—will influence the MSPA results, including the edge and perforation width, the maximum size of the islet, and the minimum size of the core [70]. For a given sufficient edge width, a higher spatial resolution and size parameter will retain more spatial detail and information of the MSPA maps [71]. To better identify the seven MSPA classes, 2-m spatial resolution, size parameter value of 7, and eight-neighbor connectivity were used in this study, reflecting the different morphological patterns of green space at the central city-scale [72] (Fig. 3b). Finally, seven non-overlapping MSPA classes (e.g., core, islet, perforation, edge, loop, bridge, and branch) were obtained (Fig. 3). The seven MSPA classes indicate the different morphological patterns of green space and have specific ecological meanings and spatial attributes (Table 2).

Green space morphological patterns were measured using the seven MSPA classes, which were indicated by the proportion of the respective MSPA class area in the grid area [73]. The area of the corresponding MSPA class was increased with the increase of the proportion. For each grid scale, the calculation of the seven MSPA classes can be expressed with Equation (1).

$$MSPA_i = S_i / S \times 100\% \tag{1}$$

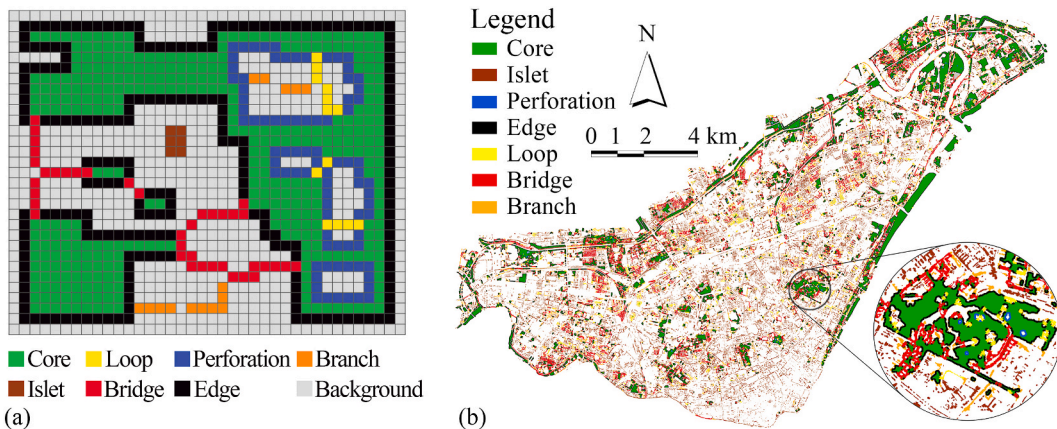
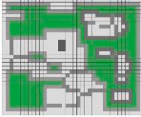
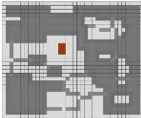
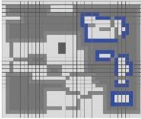

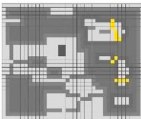
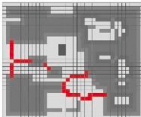
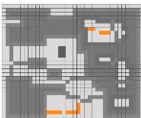


Fig. 3. Illustration of the seven MSPA classes (a) and the MSPA results in Hankou (b).

Table 2
Characteristics of the seven MSPA classes.

MSPA classes	Illustration	Characteristics
Core		Interior of a green patch with large size, such as park green space or a community park of a particular scale
Islet		The small green patches that are isolated from each other, such as scattered street trees and pocket parks
Perforation		Internal perimeters of the core class
Edge		External perimeters of the core class
Loop		Linear green space connected to the same core class, such as road greenbelt, landscape belt
Bridge		Linear green space connected to the adjacent core class
Branch		Linear green space connected at one end to perforation, edge, loop, or bridge

where $i = 1-7$, stands for the seven MSPA classes. S_i is the area of the i -th MSPA class (m^2), and S is the area of a grid (m^2).

For each scale, the overall quantity and spatial distribution characteristics of each MSPA class were presented. The $MSPA_i$ value in all grids was showed in the form of a box plot. The specific spatial distribution of the $MSPA_i$ value in each grid was displayed through colors of different shades.

2.3.2. LST retrieval

In accordance with the radiometric calibrated Landsat-7 and Landsat-8 imageries, LST was retrieved from an enhanced thematic mapper sensor (ETM+) that was mounted within the Landsat-7 satellite and a thermal infrared remote sensor (TIRS) that was mounted within the Landsat-8 satellite. LST was retrieved using radiative transfer equation, i.e., a mature and standard retrieval method [74, 75]. Landsat-7 inversion was performed using Band 6. Since the calibration parameters of TIRS 11 band were not stable, and the band was located in a high atmospheric absorption region, TIRS 10 (resampling to 30 m) was employed for inversion. Accordingly, LST with 30 m spatial resolution was determined. The specific inversion steps are expressed as follows.

1) Calculation of land surface emissivity

Land surface emissivity was accurately calculated with Equations (2)–(4).

$$E_w = 0.995 \tag{2}$$

$$\varepsilon_s = 0.9625 + 0.0614F_v - 0.0461F_v^2 \quad (3)$$

$$\varepsilon_m = 0.9589 + 0.086F_v - 0.0671F_v^2 \quad (4)$$

where F_v is the vegetation fraction. E_w , ε_s , and ε_m are the emissivity of the water body, natural surface (soil), and human-made surface (e.g., building, road), respectively.

2) Calculation of blackbody radiance

Blackbody radiance can be expressed with Equation (5).

$$B(T_s) = [L_\lambda - L_\uparrow - \tau(1-\varepsilon)L_\downarrow]/\tau\varepsilon \quad (5)$$

where $B(T_s)$ denotes the blackbody radiance derived from Planck's law; L_λ represents the spectral radiance of thermal infrared radiation received by satellite sensor ($\text{W}\cdot\text{m}^{-2}\cdot\mu\text{m}^{-1}\cdot\text{sr}^{-1}$); ε expresses land surface emissivity. L_\uparrow , L_\downarrow , and τ represent aggregated values (i.e., radiances of atmospheric upward and downward, and the transmittance of the atmosphere in the thermal infrared band, respectively). Their values were determined using the imaging time and the longitude and latitude of the imagery in accordance with NASA website (<http://atmcorr.gsfc.nasa.gov/>). In this study, L_\uparrow reached 3.93, 4.54, and 4.40 ($\text{W}\cdot\text{m}^{-2}\cdot\mu\text{m}^{-1}\cdot\text{sr}^{-1}$) in 2006, 2013, and 2018, respectively, L_\downarrow reached 5.85, 6.86, and 6.46 ($\text{W}\cdot\text{m}^{-2}\cdot\mu\text{m}^{-1}\cdot\text{sr}^{-1}$), respectively, while τ reached 0.55, 0.47, and 0.46, respectively.

3) Calculation of LST

In accordance with the inverse function of Planck's formula, the LST of centigrade was obtained after conversion with Equation (6).

$$T_s = k_2/\ln[k_1/B(T_s) + 1] - 273.15 \quad (6)$$

where T_s is the LST ($^{\circ}\text{C}$), k_1 and k_2 are the calibration constant 774.89 ($\text{W}\cdot\text{m}^{-2}\cdot\mu\text{m}^{-1}\cdot\text{sr}^{-1}$) and 1321.08 (K) for TIRS 10, and 666.09 ($\text{W}\cdot\text{m}^{-2}\cdot\mu\text{m}^{-1}\cdot\text{sr}^{-1}$) and 1282.71 (K) for ETM+ 6.

4) Validation of LST

Based on the method employed by An et al. [76], the observed air temperature and the retrieved LST were compared to verify the precision of LST. The observed air temperature was derived from eteomanz.com, where data by hours and history data can be obtained. However, there is only one alternative meteorological station in the study area (Fig. 1). The retrieved LST of the pixel where the station located was extracted, and the average value of retrieved LST from the 5×5 pixels close the station was obtained for a better comparison of the observed air temperature and the retrieved LST [76]. The time of observed air temperature was determined in accordance with the satellite transit time (GMT 3:00 in 2006, 2013, and 2018) (Table 3). The comparison results suggested that LST was usually higher than air temperature. The results of this study were also consistent with the regression model built by An et al. [76]. Thus, retrieved LST is reliable and can be employed for analysis in this study.

2.4. Statistical analysis

Four extensively employed analysis scales were proposed based on previous research to investigate the spatiotemporal effect of green space morphological patterns on LST. However, existing research has focused on the spatial non-stationarity in the correlations between green space/land cover and LST, using GWR, spatial lag model, or spatial error model [59,60]. Temporal effects of independent variables on dependent variables were not covered in the above-mentioned methods. Despite several studies covering multiple periods, the above-described methods were employed for analysis in terms of the respective period [19,41,64]. Limited studies have examined the effect from both spatial and temporal perspective. Although Hasan et al. [77] analyzed that urban green space mediated spatiotemporal variation in LST for 19 periods, they adopted Pearson's correlation to reveal the correlation between green space indicators and LST. An appropriate method is required to explore the in-depth spatiotemporal effect of green space on LST. Accordingly, GTWR was developed to reveal the spatiotemporal influence mechanism in this study. On that basis, the spatial and temporal effects will be considered.

Table 3
Comparison between retrieved LST and observed air temperature.

Year	2006	2013	2018
Observed air temperature ($^{\circ}\text{C}$)	33.2	35.1	29.2
Retrieved LST in a pixel ($^{\circ}\text{C}$)	34.4	35.1	32.3
Retrieved LST in 5×5 pixels ($^{\circ}\text{C}$)	32.6	35.2	32.4

2.4.1. Analysis scale

Since the spatial resolution of the extracted green space (0.8 m) and retrieved LST (30 m) are different, a unified spatial scale should be defined to investigate the correlation between the morphological patterns of green space and LST. As indicated by the existing research on the effects of green space on LST [36,78–80], four spatial scales (i.e., grids of 960 m, 720 m, 480 m, and 240 m) served as the appropriate scales and were adopted to unitize the two data spatially, such that the scale effects of green space morphological patterns on LST were synthetically examined.

2.4.2. Multicollinearity test

The multicollinearity of independent variables should be analyzed before the model building process, so as to ensure the rationality of the regression model. The multicollinearity test was carried out for the four grid scales. Variance inflation factor (VIF) refers to an indicator that has been extensively employed to detect multicollinearity between independent variables. It was employed to perform a collinearity test on the correlation between LST and MSPA classes in this study, such that the regression analysis results can be avoided from being affected. The larger the VIF, the greater the possibility of collinearity between independent variables. A VIF value of less than 10 suggested that the corresponding independent variables were not highly collinear, and regression analysis can be conducted directly [81].

2.4.3. Spatial auto-correlation analysis

LST was resampled by calculating the mean LST in the respective grid at the four spatial scales. Since LST usually exists spatial heterogeneity [82], spatial auto-correlation analysis should be conducted to gain more insights into the spatial patterns of LST and the effects of green space in geographical space [75,83]. The degree of spatial auto-correlation for the LST was tested using Moran's I , a widely applied geospatial correlation index [84]. Global Moran's I was first calculated based on ArcGIS 10.7 software to determine whether and to what extent spatial auto-correlation exists in the LST. The Global Moran's I value ranged from -1 to 1 . A positive value and a negative value indicated the clustering and dispersion distribution of LST, respectively, and no spatial auto-correlation was detected with a Global Moran's I value of 0 . Subsequently, Local Moran's I was obtained to find the cluster locations of low LST areas with lower LST and surrounded by grids with lower LST and vice versa (high LST clusters). The Local Moran's I value was visualized as high-high cluster, low-low cluster, high-low outlier, or low-high outlier of LST in the grids. The global and local Moran's I values were calculated with Equations (7) and (8), respectively.

$$I_g = \frac{\sum_{i=1}^n \sum_{j=1}^n W_{ij} (x_i - \bar{x})(x_j - \bar{x})}{\left(\sum_{i=1}^n \sum_{j=1}^n W_{ij} \right) \sum_{i=1}^n (x_i - \bar{x})^2} \quad (7)$$

$$I_i = x_i \sum_{j=1, j \neq i}^n w_{ij} x_j \quad (8)$$

where I_g and I_i are the global and local Moran's I , respectively; n refers to the number of the grid; x_i, x_j represent the spatial position of the grid i, j , respectively, and W_{ij} and w_{ij} are the spatial weight between grid i and j and its standardized value, respectively.

2.4.4. Regression analysis

OLS, GWR, and GTWR models at different spatial scales were built for empirical analysis on the LST and green space. The data of the dependent variable and seven independent variables were normalized prior to the building of the three models to compare the regression coefficients of the respective independent variable. Based on the comparison of the goodness of three types of models, whether the GTWR model is the optimal model for processing multi-period LST and green space data can be determined.

The OLS is a commonly used traditional linear regression model, which estimates model parameters in a global perspective, and cannot reflect the spatial non-stationarity of each parameter. The OLS model can be expressed with Equation (9):

$$y_i = \beta_0 + \sum_k \beta_k x_{ik} + \varepsilon_i \quad (9)$$

where y_i is the LST ($^{\circ}\text{C}$) of the i th grid, x_{ik} is the k th independent variable, β_k is the regression parameter of the k -th predictor variable, β_0 is the regression constant, and ε_i is the random error of a grid i .

The GWR is an improved model based on the OLS model. It applies the spatial weight matrix to the regression model, so as to better show the spatial non-stationarity of regression parameters. The GWR model can be expressed with Equation (10):

$$y_i = \beta_0(u_i, v_i) + \sum_k \beta_k(u_i, v_i) x_{ik} + \varepsilon_i \quad (10)$$

where y_i is the LST ($^{\circ}\text{C}$) of the i -th grid, x_{ik} is the k th independent variable, (u_i, v_i) is the spatial coordinates of grid i , $\beta_k(u_i, v_i)$ is the regression parameter of the k -th predictor variable, $\beta_0(u_i, v_i)$ is the regression constant, and ε_i is the random error of a grid i .

For a specific grid, distant grids have less weighting than those located nearby. This geographical weighting was implemented using a fixed Gaussian kernel. Considering there were four analysis scales in this study, corrected Akaike information criterion (AICc) was used to set bandwidth, which can search for the best distance or the number of adjacent features.

The GTWR makes up for the limitation of GWR, which only considers the spatial effect. It can reflect the temporal variation of

variable data and capture the temporal and spatial heterogeneity of variable data. The GTWR can be expressed with Equation (11):

$$y_i = \beta_0(u_i, v_i, t_i) + \sum_k \beta_k(u_i, v_i, t_i) x_{ik} + \varepsilon_i \tag{11}$$

where y_i is the LST ($^{\circ}\text{C}$) of the i -th grid, x_{ik} is the k th independent variable, i ranges from 1 to n , representing the number of grids, (u_i, v_i, t_i) is the spatiotemporal coordinates of grid i , $\beta_k(u_i, v_i, t_i)$ is the regression parameter of the k -th predictor variable, $\beta_0(u_i, v_i)$ is the regression constant, and ε_i is the random error of a grid i .

In this model, a fixed Gaussian kernel was applied and the bandwidth was set using AICc. The ratio of spatiotemporal distance parameters was set to 1.

AICc and R^2 were proposed in accordance with existing research to compare the fitting effect between GTWR, GWR, and OLS [62]. A lower AICc value and a higher R^2 value can indicate a better fitting effect of a model. $\text{Adj.}R^2$ denotes the adjusted R^2 , eliminating the influence of the sample size difference on the fitting degree in a wide variety of spatial scale models. The three types of regressions were executed with ArcGIS 10.7.

2.4.5. Data statistical

First, the mean, the minimum, the maximum and the quartile were adopted to express the regression coefficient of the GTWR model. Second, the frequency and spatiotemporal distribution of the coefficient of the respective variable were plotted respectively. The 0 was set as an interval value to distinguish positive and negative coefficients. As indicated by a negative coefficient, the MSPA class can facilitate the cooling process, while a positive coefficient means an opposite effect. The effect was increased with the rise of the absolute value of the coefficient.

3. Results

3.1. Spatial pattern of green space and LST

3.1.1. Spatial characteristics of green space morphological patterns

The quantity of green space was significantly close in the first two years. However, in 2013 and 2017, significant differences were found between seven MSPA classes (Fig. 4). At the grid scale of 960 m, despite the increase of the area of green spaces, the general spatial pattern of the green spaces showed a fragmented distribution. The proportion of the core declined significantly, and the proportion of the islet was elevated notably from 2013 to 2017. According to the total proportion of the seven MSPA classes in the entire study area, the core was the first dominant MSPA class in 2006 and 2013, which mainly consists of a certain number of urban park green spaces, ecological green spaces, and attached green spaces. However, the islet became the first dominant MSPA class in 2017. At the other three scales, the spatial pattern of green spaces exhibited similar characteristics (Tables S1–S3).

As for spatial distribution characteristics of MSPA classes, the same MSPA class was similar, but there were significant differences between different MSPA classes (Figs. S1–S3). The core and edge accounted for a high proportion along the fringe of the site and in the urban park green space zones, respectively. The islet and branch proportion were similar in high values scattered among most areas of the entire site. Likewise, the high values of loop and bridge proportion were dispersed in the site exhibiting a lower density. The perforation, displaying a similar spatial pattern to that of the core, accounted for the lowest proportion.

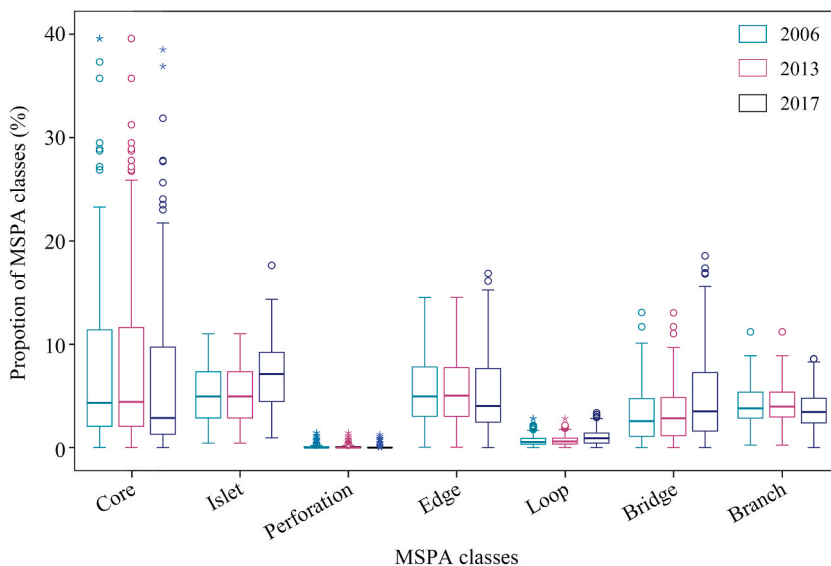


Fig. 4. Proportion of the seven MSPA classes in the three years at the scale of 960 m.

3.1.2. The spatial pattern of LST

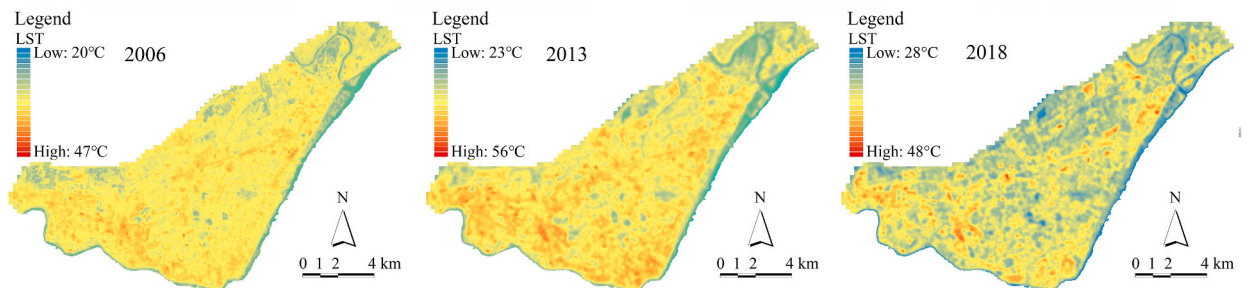
In general, the LST of Hankou reached its maximum in 2013 and its minimum in 2006 (Fig. 5). The above trend was consistent with the fluctuation of the air temperature when the three Landsat satellites were acquired in accordance with the national meteorological station in Wuhan.

Despite different LST ranges reported in three periods, the LST spatial patterns were similar (Fig. 5a). As depicted in Fig. 5b, several low-temperature zones were primarily located in the north areas. In contrast, the high-temperature zones scattered in the study area mostly lacked green space and primarily comprised impervious surfaces.

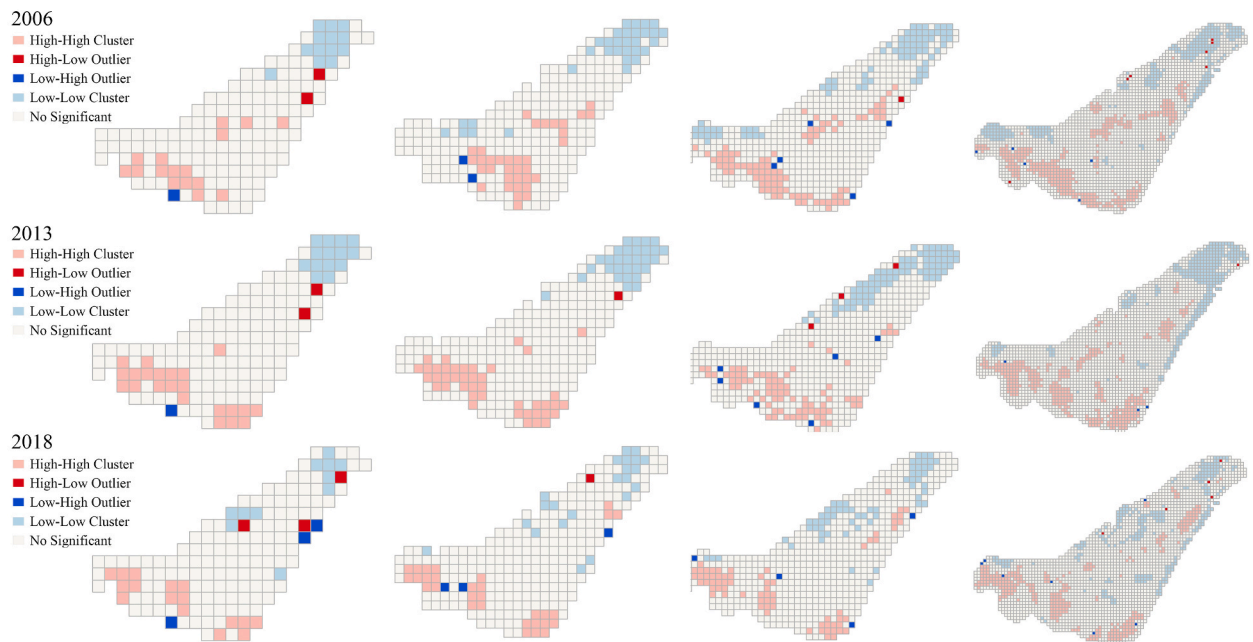
In general, LST of the four spatial scales exhibited significant positive spatial auto-correlation in three years ($p < 0.0001$) (Table 4). Besides, the spatial auto-correlation became more significant at a smaller scale. As Fig. 5b shown, at the scale of 960 m, the high LST clusters were distributed in the southwest of Hankou, and the low LST clusters were located in the northeast corner. The site encompassed one grid with high LST surrounded by low LST and two grids with low LST surrounded by high LST. With the decrease in the spatial scale, the grids around the second ring road in the middle of Hankou were identified with high LST clusters and the grids along the eastern shoreline and between the third and second ring roads exhibited low LST clusters. Furthermore, the high-low outlier and low-high outlier of LST tended to disappear.

3.2. Regression model comparison

As indicated by the result of the multicollinearity test, the seven independent variables (MSPA classes) did not exhibit multicollinearity at the four scales. As Table S4 shows, GTWR model can better explain the data with spatiotemporal characteristics and the impact of MSPA classes on the LST. With GTWR models, most MSPA classes can account for more than 80 % of LST variance. The scales



(a) LST maps in the three years



(b) Spatial auto-correlation analysis of LST at the four scales

Fig. 5. LST maps in the three years (a) and their spatial auto-correlation analysis at the four spatial scales (b).

Table 4
Global Moran's *I* of LST at different scales.

Scale	240 m	480 m	720 m	960 m
2006	0.70	0.66	0.55	0.42
2013	0.74	0.56	0.58	0.48
2018	0.63	0.51	0.46	0.33

of 960 m for the MSPA classes were found for the most likely alternative scale to explain LST variance.

3.3. Spatiotemporal characteristics of regression coefficients of GTWR model

As Fig. 6 shown, the respective MSPA class showed different effects on LST and their regression coefficients had certain differences at the four scales. In general, the core was negatively correlated with LST. Notably, the maximum regression coefficient of the core was negative at the 960 m and 240 m scale (Fig. 6a and d). In contrast, the islet was positively correlated with LST. The coefficient of the perforation displayed a multi-peak distribution while playing an opposite role at the large scale and small scale (Fig. 6a and c), with the main peak greater than 0 or close to 0. The edge almost adversely affected LST in addition to 960 m scale. The main peaks of coefficients of the loop were close to 0 and the frequency of negative and positive value was similar, suggesting loop's complicated effects on LST. The bridge almost adversely affected LST. The branch was also dominated by cooling effects except at the 720 m scale (Fig. 6b).

As Fig. 7 shown, grids with red color represent positive coefficients (warming effect) and blue color for negative coefficients (cooling effect). Because variables were normalized, the above-described coefficients can be compared and can reflect the extent of their contribution. Given display quality of other three smaller scales and, their regression coefficients were displayed in Tables S5–S7. The table contains longitude and latitude coordinates of the respective grid center.

Regression coefficients of the seven MSPA classes notably varied from different grids and different periods in Hankou. At the first

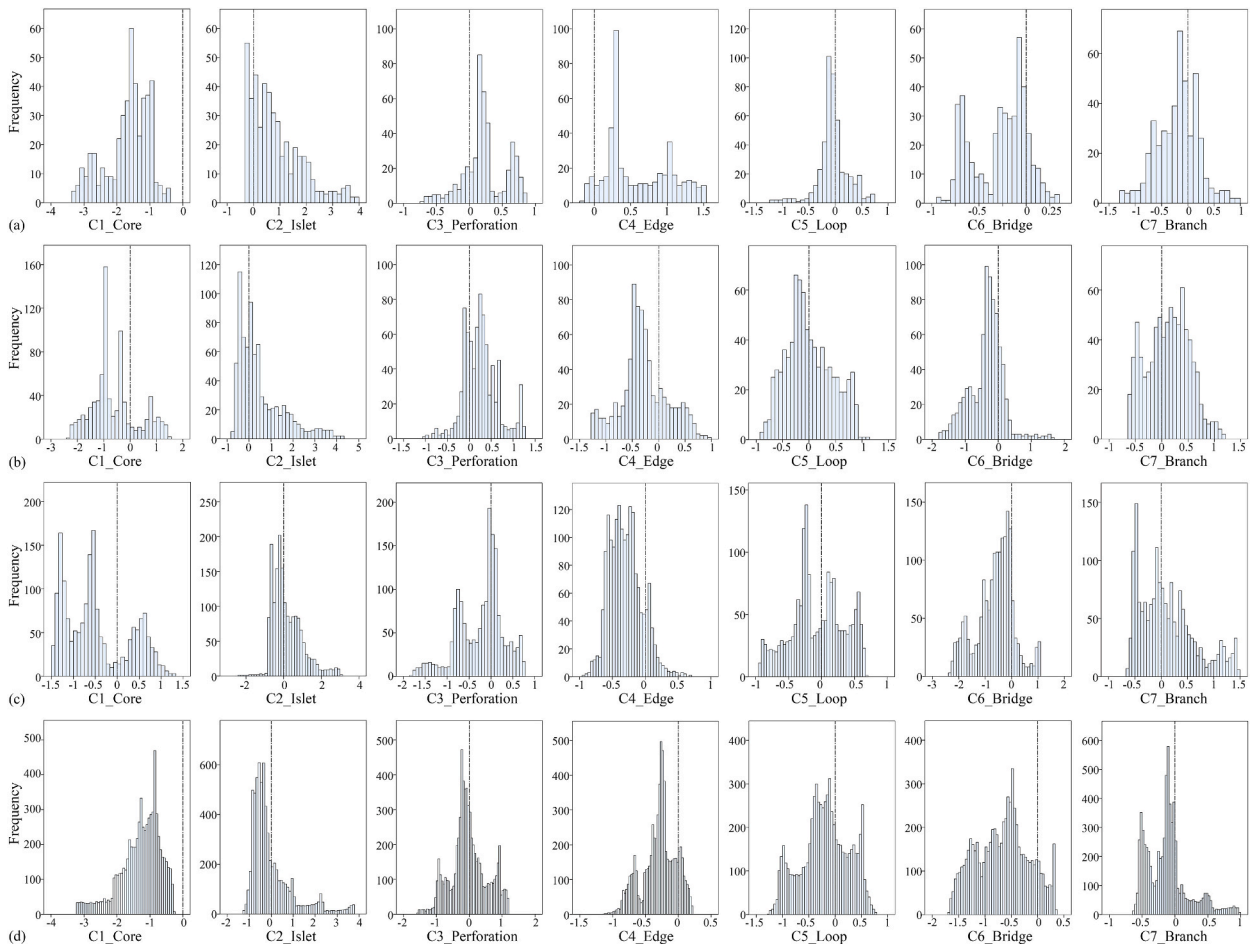


Fig. 6. Frequency of regression coefficients of each variable at the scale of 960 m (a), 720 m (b), 480 m (c), and 240 m (d).

stage (2006) (Fig. 7), the core in all grids adversely affected LST, and the islet exerted warming effects. The most substantial cooling effects of the core were located in the south and middle corners, respectively. Besides, the islet exhibited the most impact strength in the north and west corners. The coefficients of the perforation and edge were dominated by positive values. Most coefficient values of the perforation were small. The edge displayed a distribution pattern with higher coefficients in the east and north, and it had barely effects on LST in the west. The loop, the bridge, and the branch (i.e., three types of linear MSPA classes) achieved small coefficient values. The bridge exerted a slight cooling effect in the middle and south corners, and the branch exerted this effect in the west and south corners. The coefficients of the loop varied from negative to positive from north to south.

In 2013, the bridge in all grids had adversely affected LST. The trend of the coefficients of the other six MSPA classes was consistent with that in 2006. At the third stage, the core contributed the most to LST in the whole region, and the impact strength of the islet decreased. However, the negative coefficient of the branch and perforation increased in the west. The above-mentioned phenomena indicate spatiotemporal differences of the influence of MSPA classes on LST.

In addition, the south corner, the densest area in Hankou, exhibited the highest frequency of a considerable negative coefficient value, suggesting that a small increase in the MSPA class proportion can lead to a significant decrease in LST. The LST regulation effect

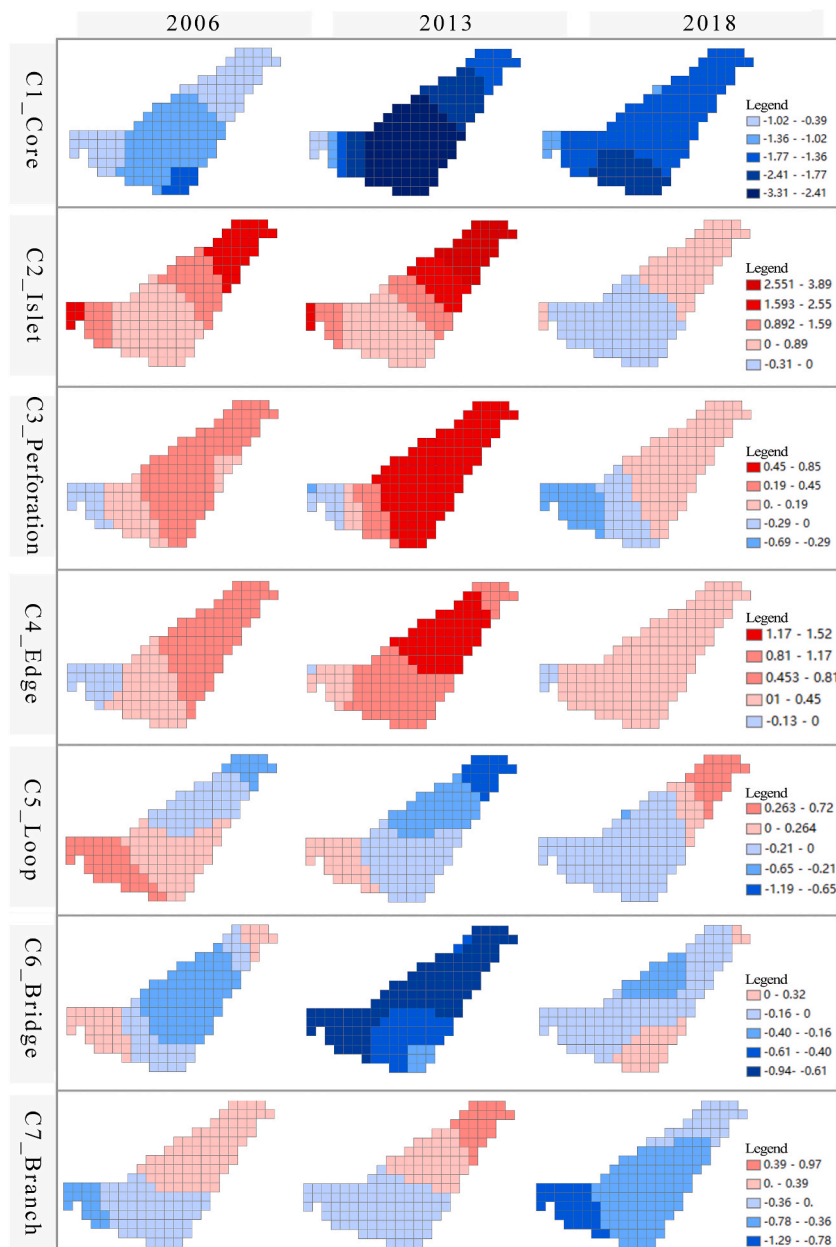


Fig. 7. Regression coefficients of the GTWR for the seven MSPA classes at the spatial scales of 960 m in the three years.

of green space was dominated by cooling. In the north area, the green space area was relatively large. The increase of the islet also led to the increase of LST. Except for the islet, although a positive coefficient of the other MSPA classes was observed in some grids, they usually achieved small values.

4. Discussion

This study makes contributions to neighborhood-level green space planning and design for the thermal environment improvement. First, although significant were found between spatial patterns of green space measured by landscape metrics, this study used MSPA to further explore the relationship between green space pattern and LST in a new way, which can provide visual images of different green space classes to guide the optimization of green space morphological pattern in a spatially explicit way. Second, to our knowledge, this study may be the first to test the spatiotemporal influence of green space pattern on LST using GTWR models, which consider both spatial and temporal non-stationarity of the influence.

4.1. Influence of MSPA classes on LST

Among the various types of urban land cover, green space usually considered one of the most efficient factors for LST regulation [7, 16]. Mumtaz et al. [85] suggested that conversion from vegetation into built-up or barren lands resulted in the increase in LST. However, given the complex relationship among the above-described land cover factors, it is difficult to completely eliminate the influence of other factors in an empirical study. Thus, this study placed a focus on green space. As Lin et al. found that the core, perforation, loop of green space exerted huge influences on heat island intensity [51], in this study, there were significant relationships between seven MSPA classes and LST. In the study conducted by Xie et al. [41], the OLS composed of five samples revealed that increasing areas of all the seven MSPA classes resulted in cooling the environments. In particular, the edge, bridge, and branch had a significant influence. However, our results add the dimensions of the relationship between these indicators and LST. The effects of seven MSPA classes showed vast differences. Some influence rules can be summarized based on the frequency maps.

As revealed by the lower proportions of the positive regression coefficient of the core in GTWR, a higher proportion of the large green space patch in a specific area can be conducive to mitigating LST, consistent with the relationship between the landscape metric LPI [29], thus suggesting the most massive green patch in a green space. A larger green space had a better cooling benefit since more tree canopies and leaf areas or densities can be used for solar radiation interception and shading [86,87]. The cluster of trees also increased the roughness of the surface, enhancing local air circulations or inversions [8], which can contribute to heat removal. Besides, the cooling effect of extensive green space can extend to its surrounding areas, and the green space with a more substantial area or tree canopy generally exhibits a longer cooling distance and a higher cooling intensity [88–90], such that more LST can be effectively reduced. As the internal boundary of the core, Xie et al. [41] suggested that perforation keeps thermal environments stable most effectively. However, in this study, the spatial non-stationarity of the influence of this index on LST was proposed. We found that an increase in the perforation's proportion led to an increase in LST in most area, probably due to the damage of the integrity of the core.

The islet was dominated by a warming effect, because the area was too small for the islet to generate cooling benefits [91], such that the LST tended to be increased. Forman [92] has suggested that the fragmented distribution of green space will result in low LST, primarily arising from the increase of the shade area and the interaction between green spaces and their surrounding areas. It dependent on the vegetation type and its canopy; trees with small canopies exerted a warming effect [93], suggesting that the area of green space should reach a certain threshold containing sufficient leaf area [94].

The edge's influence on LST presented a scale difference. On the one hand, the edge consistently showed a negative relationship with LST at the scale of 720 m and 480 m, consistent with the existing research that LST was lower in an area with a higher ED due to more areas of shade [95]. The edge proportion in this study reflected the dispersion of the core, thus contributing to the cooling process due to a sufficient area despite high scatter [94]. On the other hand, an opposite result was found at the scale of 240 m, consistent with the research of Masoudi and Tan [24] using the same spatial scale of 240 m, reported a positive relationship between the ED and LST. The possible reason is that under a constant green space area, a large ED indicated a high fragmentation of the green space. Accordingly, there were usually a considerable number of small green patches, such that an ineffective cooling effect was generated.

As a green belt connecting two large green patches, the bridge mainly showed a cooling effect, suggesting that the bridge with a higher proportion tended to have a lower LST. The bridge closely links the relationship among different green patches, undertaking the function of an urban ecological corridor. The strong cooling effect of green belt space at the block scale was confirmed in this study. Through ENVI-met simulation, Sodoudi et al. [93] showed that belt green spaces with a more stretched shape had better cooling effects. The above-mentioned phenomena may be due to the ecological benefits of their linear morphology that can more effectively penetrate surrounding areas [96]. The positive and negative frequency of the loop and branch was similar. On the one hand, the loop increases the connectivity within the green space. On the other hand, with the increase in the proportion of the loop, it also weakens the area of the core to a certain extent, leading to the increase in LST. The warming effect of the branch may be due to its morphology extending from the core or other MSPA classed, which is exposed to the hard surface. Accordingly, an area with too high proportion of the branch is not conducive to the decrease of LST of the green space.

4.2. Implications of spatiotemporal non-stationarity, spatial scale effect, and green space strategies

The GTWR model shows a significant advantage that its regression coefficients indicate the spatiotemporal variation characteristics

of the influence of MSPA classes on LST. For instance, at the scale of 960 m, nearly 74 % of the grid had a coefficient derived from the GTWR model less than that in the OLS model (-1.933), suggesting that the effect of increasing the core proportion on LST would be overestimated for about 74 % of the study site if using an OLS model. Notably, there were 26 % of the area with an enhanced cooling effect of increasing the core on LST.

The spatiotemporal patterns of the coefficient derived from GTWR models can provide correct information to guide LST reduction and raise appropriate planning strategies. The negative relationships between MSPA classes (mainly the core) and LST were influential in the densely built area (e.g., the south corner in Hankou), suggesting that a small increase in MSPA proportion in such areas leads to a more significant reduction in LST compared with elsewhere. However, there were many positive regression coefficients for the islet. The positive relationship was considerably strong in the north and west corners close to urban fringes, suggesting that a small increase in the islet in such areas can lead to a more considerable increase in LST compared with elsewhere. Accordingly, the green space of different morphological patterns was preferentially arranged in the high-density areas of this study site, while the fragmentation of green space in fringe areas was avoided, and small-sized green patches were formed.

The spatial auto-correlation of LST and its relationship with MSPA classes were affected by the statistic grid-scale. In GTWR models, the R^2 reached its peak at the 960 m scale, suggesting the scale-dependence for green space morphological pattern optimization in the neighborhood. In China, 960 m refers to the scale that defines the neighborhood, i.e., the range between 800 m and 1200 m composed of urban trunk roads. Consequently, the relationship between the MSPA-based morphological pattern of green space and LST can be examined at the 960 m grid more effectively. Although 960 m may not serve as an optimal scale, a neighborhood scale should be employed as a basic unit for green space adjustment strategies in an ordinary urban neighborhood under the general planning of green space system.

Inconsistent with landscape metrics analysis, MSPA can be more effectively employed in green space management based on the visualized distribution of green space with different morphological patterns. To be specific, the quantity, spatial pattern, and location of the green space can be conclusively determined. Different MSPA classes can transform each other. It is noteworthy that the islet can be transformed into the branch or core through its expansion if possible. On that basis, a MSPA-based green space micro-network should be developed, which is dominated by a large green patch and connected with the surrounding small-to-medium-sized green patches via a green belt. A simulation study on green space network planning to optimize the thermal environment has suggested that a comprehensive organization of green patches and corridors will exert a better cooling effect than that of a single spatial element of green space [97]. Since increasing a sizeable green space may be limited in urban high-density areas, the small-to-medium-sized green space should be increased maximally, which can be adopted to optimize the local thermal environment. Even a small green space, a network, or a dispersion layout is also strongly recommended to across the entire area [98]. Furthermore, combined with greenway construction, streets should be fully afforested and link adjacent green patches based on the level and condition of the street. Trees with large canopies and leaf density serve as optional green spaces.

5. Conclusion

Based on the green space and LST data with 0.8 m and 30 m resolution, respectively, in the three periods, the spatiotemporal influence of morphological spatial pattern of the green space on LST was revealed through GWTR models. The findings are as follows: (1) The GTWR model of the respective MSPA class outperformed the corresponding OLS and GWR models since the considerably higher R^2 and the lower AICc value were determined from GTWR models. For GTWR models, the lowest $Adj.R^2$ was 0.808 at the 240 m scale. (2) In general, the core, the edge, the bridge, and the branch achieved negative coefficients, and the islet achieved a positive coefficient. However, the perforation and the loop exerted significant dual nature effects with the similar quantity of the negative and positive coefficients. The temporal characteristics of the influence pattern and strength of the most MSPA classes were similar in 2006 and 2013. Some differences in the spatial distribution of the regression coefficient of the edge, loop, and branch were found in 2018. (3) The intensity of the effect of the respective MSPA class varied across the study area. At the 960 m scale, the absolute value of the regression coefficient reached its highest (-3.31) and lowest (-0.02) value for the core and the edge, respectively. (4) A neighborhood scale, which was 960 m in this study, was demonstrated as a basic unit in green space management. The spatiotemporal non-stationarity of the relationships offers essential insights for urban thermal environment improvement through urban green space planning and design.

Several limitations remained in this study. The study was conducted based on LST derived from one daytime remote sensing imagery. Multi seasonal effects of green space on LST can be investigated in depth. Whether the findings can be applied to small-to-medium-sized cities or megacities in other climate zones requires multicity comparison research. In particular, further studies are required to explore whether the suggested scale (960 m) is applicable to other regions. Also, the numerical interval of multi-scale can be set smaller, so as to more finely reveal the appropriate scale. Finally, other factors, (e.g., water bodies, built-up areas, and barren land) can be controlled on a similar level for future research by thoroughly selecting research areas or using simulation methods.

Data availability statement

Data will be made available on request.

CRedit authorship contribution statement

Ming Chen: Writing – review & editing, Writing – original draft, Software, Methodology, Investigation, Funding acquisition,

Formal analysis, Data curation, Conceptualization. **Yubo Sun**: Software, Resources, Methodology, Investigation. **Bo Yang**: Validation, Supervision, Conceptualization. **Jiayi Jiang**: Writing – review & editing, Validation, Supervision, Conceptualization.

Declaration of competing interest

The authors declare that they have no known competing financial interests or personal relationships that could have appeared to influence the work reported in this paper.

Acknowledgements

This study was supported by the National Natural Science Foundation of China [grant number 52208058 and 52178041].

Appendix A. Supplementary data

Supplementary data to this article can be found online at <https://doi.org/10.1016/j.heliyon.2024.e31363>.

References

- [1] M.Y. Aslam, K.R. Krishna, G. Beig, M.I.R. Tinmaker, D.M. Chate, Diurnal evolution of urban heat island and its impact on air quality by using ground observations (SAFAR) over New Delhi, *Open J. Air Pollut.* 6 (2) (2017) 52–64.
- [2] F. Kong, C. Sun, F. Liu, H. Yin, F. Jiang, Y. Pu, G. Cavan, C. Skelhorn, A. Middel, I. Dronova, Energy saving potential of fragmented green spaces due to their temperature regulating ecosystem services in the summer, *Appl. Energy* 183 (2016) 1428–1440.
- [3] R. Kotharkar, A. Ramesh, A. Bagade, Urban heat island studies in south Asia: a critical review, *Urban Clim.* 24 (2018) 1011–1026.
- [4] N. Mazhar, R.D. Brown, N. Kenny, S. Lenzholzer, Thermal comfort of outdoor spaces in Lahore, Pakistan: lessons for bioclimatic urban design in the context of global climate change, *Landsc. Urban Plann.* 138 (2015) 110–117.
- [5] C. Alexander, Normalised difference spectral indices and urban land cover as indicators of land surface temperature (LST), *Int. J. Appl. Earth Obs. Geoinf.* 86 (2020) 102013.
- [6] D. Armson, P. Stringer, A.R. Ennos, The effect of tree shade and grass on surface and globe temperatures in an urban area, *Urban For. Urban Green.* 11 (2012) 245–255.
- [7] D.E. Bowler, L. Buyung-Ali, T.M. Knight, A.S. Pullin, Urban greening to cool towns and cities: a systematic review of the empirical evidence, *Landsc. Urban Plann.* 97 (3) (2010) 147–155.
- [8] T.R. Oke, J.M. Crowther, K.G. McNaughton, J.L. Monteith, B. Gardiner, The micrometeorology of the urban forest, *Philos. Trans. R. Soc. B-Biol. Sci.* 342 (1989) 335–349.
- [9] N. Kabisch, D. Haase, Green spaces of European cities revisited for 1990–2006, *Landsc. Urban Plann.* 110 (2013) 113–122.
- [10] P. Cohen, O. Potchter, A. Matzarakis, Daily and seasonal climatic conditions of green urban open spaces in the Mediterranean climate and their impact on human comfort, *Build. Environ.* 51 (2012) 285–295.
- [11] A. Hami, B. Abdi, D. Zarehaghi, S.B. Maulan, Assessing the thermal comfort effects of green spaces: a systematic review of methods, parameters, and plants' attributes, *Sustain. Cities Soc.* 49 (2019) 101634.
- [12] D. Lai, Y. Liu, M. Liao, B. Yu, Effects of different tree layouts on outdoor thermal comfort of green space in summer Shanghai, *Urban Clim.* 47 (2023) 101398.
- [13] L.L.H. Peng, Z. Jiang, X. Yang, Y. He, T. Xu, S.S. Chen, Cooling effects of block-scale façade greening and their relationship with urban form, *Build. Environ.* 169 (2020) 106552.
- [14] H. Tang, J. Liu, B. Zheng, Study on the green space patterns and microclimate simulation in typical urban blocks in central China, *Sustainability* 14 (22) (2022) 15391.
- [15] Q. Zhang, D. Zhou, D. Xu, J. Cheng, A. Rogora, Influencing factors of the thermal environment of urban green space, *Heliyon* 8 (11) (2022) e11559.
- [16] P. Lin, S.S.Y. Lau, H. Qin, Z. Gou, Effects of urban planning indicators on urban heat island: a case study of pocket parks in high-rise high-density environment, *Landsc. Urban Plann.* 168 (2017) 48–60.
- [17] A. Solcerova, F. van de Ven, M. Wang, M. Rijdsdijk, N. van de Giesen, Do green roofs cool the air? *Build. Environ.* 111 (2017) 249–255.
- [18] Z. Li, H. Zhang, Y.H. Juan, et al., Effects of urban tree planting on thermal comfort and air quality in the street canyon in a subtropical climate, *Sustain. Cities Soc.* 91 (2023) 104334.
- [19] Y. Cai, Y. Chen, C. Tong, Spatiotemporal evolution of urban green space and its impact on the urban thermal environment based on remote sensing data: a case study of Fuzhou City, China, *Urban for, Urban Green.* 41 (2019) 333–343.
- [20] J. Yang, J. Sun, Q. Ge, X. Li, Assessing the impacts of urbanization-associated green space on urban land surface temperature: a case study of Dalian, China, *Urban for, Urban Green.* 22 (2017) 1–10.
- [21] M. Zhang, F. Zhang, D. Chen, M.L. Tan, N.W. Chan, Urban local surface temperature prediction using the urban gray-green space landscape and vegetation indices, *Build. Environ.* 226 (2022) 109723.
- [22] T. Kubota, H.S. Lee, A.R. Trihamdani, T.T.P. Tran, T. Tanaka, K. Matsuo, Impacts of land use changes from the Hanoi Master Plan 2030 on urban heat islands: Part 1. cooling effects of proposed green strategies, *Sustain. Cities Soc.* 32 (2017) 295–317.
- [23] W. Jia, S. Zhao, Trends and drivers of land surface temperature along the urban-rural gradients in the largest urban agglomeration of China, *Sci. Total Environ.* 711 (2020) 134579.
- [24] M. Masoudi, P.Y. Tan, Multi-year comparison of the effects of spatial pattern of urban green spaces on urban land surface temperature, *Landsc. Urban Plann.* 184 (2019) 44–58.
- [25] L. Yao, T. Li, M. Xu, Y. Xu, How the landscape features of urban green space impact seasonal land surface temperatures at a city-block-scale: an urban heat island study in Beijing, China, *Urban for, Urban Green.* 52 (2020) 126704.
- [26] Z. Yu, G. Yang, S. Zuo, G. Jørgensen, M. Koga, H. Vejre, Critical review on the cooling effect of urban blue-green space: a threshold-size perspective, *Urban For. Urban Green.* 49 (2020) 126630.
- [27] D. Chen, F. Zhang, M. Zhang, Q. Meng, C.Y. Jim, J. Shi, M.L. Tan, X. Ma, Landscape and vegetation traits of urban green space can predict local surface temperature, *Sci. Total Environ.* 825 (2022) 154006.
- [28] L. Feng, M. Zhao, Y. Zhou, L. Zhu, H. Tian, The seasonal and annual impacts of landscape patterns on the urban thermal comfort using Landsat, *Ecol. Indic.* 110 (2020) 105798.
- [29] Y. Liu, J. Peng, Y. Wang, Efficiency of landscape metrics characterizing urban land surface temperature, *Landsc. Urban Plann.* 180 (2018) 36–53.

- [30] R. Lyu, J. Pang, X. Tian, W. Zhao, J. Zhang, How to optimize the 2D/3D urban thermal environment: insights derived from UAV LiDAR/multispectral data and multi-source remote sensing data, *Sustain. Cities Soc.* 88 (2023) 104287.
- [31] S. Pramanik, M. Punia, Assessment of green space cooling effects in dense urban landscape: a case study of Delhi, India, *Model. Earth Syst. Environ.* 5 (2019) 867–884.
- [32] J. Peng, P. Xie, Y. Liu, J. Ma, Urban thermal environment dynamics and associated landscape pattern factors: a case study in the Beijing metropolitan region, *Remote Sens. Environ.* 173 (2016) 145–155.
- [33] E.J. Wesley, N.A. Brunzell, Greenspace pattern and the surface urban heat island: a biophysically-based approach to investigating the effects of urban landscape configuration, *Rem. Sens.* 11 (19) (2019) 2322.
- [34] H. Wu, L. Ye, W. Shi, K. Clarke, Assessing the effects of land use spatial structure on urban heat islands using HJ-1B remote sensing imagery in Wuhan, China, *Int. J. Appl. Earth Obs. Geoinf.* 32 (2014) 57–78.
- [35] A. Chen, X.A. Yao, R. Sun, L. Chen, Effect of urban green patterns on surface urban cool islands and its seasonal variations, *Urban For. Urban Green.* 13 (2014) 646–654.
- [36] G. Guo, Z. Wu, Y. Chen, Complex mechanisms linking land surface temperature to greenspace spatial patterns: evidence from four southeastern Chinese cities, *Sci. Total Environ.* 674 (2019) 77–87.
- [37] T. Basu, A. Das, Urbanization induced degradation of urban green space and its association to the land surface temperature in a medium-class city in India, *Sust. Cities Soc.* 90 (2023) 104373.
- [38] S. Huang, X. Xiao, T. Tian, Y. Che, Seasonal influences on preferences for urban blue-green spaces: integrating land surface temperature into the assessment of cultural ecosystem service value, *Sustain. Cities Soc.* 102 (2024) 105237.
- [39] I. Dutta, A. Das, Quantifying the impact of urban green space pattern to land surface temperature: evidence from an urban agglomeration of Eastern India, in: *Advancements in Urban Environmental Studies: Application of Geospatial Technology and Artificial Intelligence in Urban Studies*, Springer International Publishing, Cham, 2023, pp. 161–177.
- [40] A. Das, M. Das, Exploring the relationship between quality of living and green spaces in cities: evidence from an Indian megacity region of global south, *Land Use Pol.* 129 (2023) 106594.
- [41] M. Xie, Y. Gao, Y. Cao, J. Breuste, M. Fu, D. Tong, Dynamics and temperature regulation function of urban green connectivity, *J. Urban Plan. Dev* 141 (3) (2015) A5014008.
- [42] S. Wu, D. Wang, Z. Yan, X. Wang, J. Han, Spatiotemporal dynamics of urban green space in Changchun: changes, transformations, landscape patterns, and drivers, *Ecol. Indic.* 147 (2023) 109958.
- [43] B. Li, B. Zhang, L. Yin, J. Chang, Assessing heat risk for residents of complex urban areas from an accessibility-based perspective, *Sustain. Cities Soc.* 88 (2023) 104278.
- [44] Q. Liu, M. Xie, R. Wu, Q. Xue, B. Chen, Z. Li, X. Li, From expanding areas to stable areas: identification, classification and determinants of multiple frequency urban heat islands, *Ecol. Indic.* 130 (2021) 108046.
- [45] J. Luo, H. Fu, Constructing an urban cooling network based on PLUS model: implications for future urban planning, *Ecol. Indic.* 154 (2023) 110887.
- [46] Z. Zhao, W. Li, J. Zhang, Y. Zheng, Constructing an urban heat island network based on connectivity perspective: a case study of Harbin, China, *Ecol. Indic.* 159 (2024) 111665.
- [47] L. Jiang, M. Xie, B. Chen, W. Su, X. Zhao, R. Wu, Key areas and measures to mitigate heat exposure risk in highly urbanized city: a case study of Beijing, China, *Urban Clim.* 53 (2024) 101748.
- [48] F. Liu, J. Liu, Y. Zhang, S. Hong, W. Fu, M. Wang, J. Dong, Construction of a cold island network for the urban heat island effect mitigation, *Sci. Total Environ.* 915 (2024) 169950.
- [49] B. Li, B. Zhang, L. Yin, J. Chang, Assessing heat risk for residents of complex urban areas from an accessibility-based perspective, *Sustain. Cities Soc.* 88 (2023) 104278.
- [50] J. Qiu, X. Li, W. Qian, Optimizing the spatial pattern of the cold island to mitigate the urban heat island effect, *Ecol. Indic.* 154 (2023) 110550.
- [51] J. Lin, S. Qiu, X. Tan, Y. Zhuang, Measuring the relationship between morphological spatial pattern of green space and urban heat island using machine learning methods, *Build. Environ.* 228 (2023) 109910.
- [52] J. Wu, P. Han, J. Yu, S. Jarvie, Y. Zhang, Q. Zhang, Edge grassland provide a stronger thermal buffer against core grassland in the agro-pastoral ecotone of Inner Mongolia, *Ecol. Indic.* 154 (2023) 110762.
- [53] Y. Zhang, N. Tian, A. Chen, J. Qiu, C. He, Y. Cao, Identification of a wetland ecological network for urban heat island effect mitigation in Changchun, China, *Ecol. Indic.* 150 (2023) 110248.
- [54] W. Shen, Q. Liu, M. Ji, J. He, T. He, C. Huang, Impacts of urban forests and landscape characteristics on land surface temperature in two urban agglomeration areas of China, *Sustain. Cities Soc.* 99 (2023) 104909.
- [55] M. Mansourmoghaddam, N. Naghipur, I. Rousta, S.K. Alavipanah, H. Olafsson, A.A. Ali, Quantifying the effects of green-town development on land surface temperatures (LST) (A case study at Karizland (Karizboom), Yazd, Iran), *Land* 12 (2023) 885.
- [56] C. Li, L. Lu, Z. Fu, R. Sun, L. Pan, L. Han, H. Guo, Q. Li, Diverse cooling effects of green space on urban heat island in tropical megacities, *Front. Environ. Sci.* 10 (2022) 3389.
- [57] W. Zhou, F. Cao, Effects of changing spatial extent on the relationship between urban forest patterns and land surface temperature, *Ecol. Indic.* 109 (2020) 105778.
- [58] S. Li, Z. Zhao, X. Miaomiao, Y. Wang, Investigating spatial non-stationary and scale-dependent relationships between urban surface temperature and environmental factors using geographically weighted regression, *Environ. Model. Software* 25 (12) (2010) 1789–1800.
- [59] A. Guo, J. Yang, X. Xiao, J. Xia, C. Jin, X. Li, Influences of urban spatial form on urban heat island effects at the community level in China, *Sust. Cities Soc.* 53 (2020) 101972.
- [60] J. Song, S. Du, X. Feng, L. Guo, The relationships between landscape compositions and land surface temperature: quantifying their resolution sensitivity with spatial regression models, *Landsc. Urban Plann.* 123 (2014) 145–157.
- [61] A. Guo, J. Yang, W. Sun, X. Xiao, J.X. Cecilia, C. Jin, X. Li, Impact of urban morphology and landscape characteristics on spatiotemporal heterogeneity of land surface temperature, *Sustain. Cities Soc.* 63 (2020) 102443.
- [62] Y.F. Su, G.M. Foody, K.S. Cheng, Spatial non-stationarity in the relationships between land cover and surface temperature in an urban heat island and its impacts on thermally sensitive populations, *Landsc. Urban Plann.* 107 (2012) 172–180.
- [63] W. Liu, B. Jia, T. Li, Q. Zhang, J. Ma, Correlation analysis between urban green space and land surface temperature from the perspective of spatial heterogeneity: a case study within the sixth ring road of Beijing, *Sustainability* 14 (2022) 13492.
- [64] T. Basu, A. Das, Urbanization induced degradation of urban green space and its association to the land surface temperature in a medium-class city in India, *Sust. Cities Soc.* 90 (2023) 104373.
- [65] M.A. Degefu, M. Argaw, G.L. Feyisa, S. Degefa, Dynamics of green spaces- Land surface temperature intensity nexus in cities of Ethiopia, *Heliyon* 9 (2) (2023) e13274.
- [66] J. Wang, W. Zhou, Y. Qian, W. Li, L. Han, Quantifying and characterizing the dynamics of urban greenspace at the patch level: a new approach using object-based image analysis, *Remote Sens. Environ.* 204 (2018) 94–108.
- [67] W. Lin, T. Yu, X. Chang, W. Wu, Y. Zhang, Calculating cooling extents of green parks using remote sensing: method and test, *Landsc. Urban Plann.* 134 (2015) 66–75.
- [68] R. Nemani, S. Running, Estimation of regional surface resistance to evapotranspiration from NDVI and thermal-IR AVHRR data, *J. Appl. Meteorol.* 28 (4) (1989) 276–284.
- [69] P. Soille, *Morphological Image Analysis: Principles and Applications*, second ed., Springer-Verlag, New York, 2003.

- [70] P. Vogt, K.H. Riitters, C. Estreguil, J. Kozak, T.G. Wade, J.D. Wickham, Mapping spatial patterns with morphological image processing, *Landsc. Ecol.* 22 (2007) 171–177.
- [71] K. Ostapowicz, P. Vogt, K.H. Riitters, J. Kozak, C. Estreguil, Impact of scale on morphological spatial pattern of forest, *Landsc. Ecol.* 23 (9) (2008) 1107–1117.
- [72] Y. Gao, H. Huang, Z. Li, L. Chen, T. He, Y. Zheng, Construction of the ecological network of Pingtan Island based on MSPA, *J. Fujian Agric. For. Univ. (Nat. Sci. Ed.)* 48 (5) (2019) 640–648. Available at: <http://www.cnki.com.cn/Article/CJFDTotal-FJND201905017.htm> (in Chinese).
- [73] M. Chen, F. Dai, B. Yang, S. Zhu, Effects of urban green space morphological pattern on variation of PM_{2.5} concentration in the neighborhoods of five Chinese megacities, *Build. Environ.* 158 (2019) 1–15.
- [74] J.A. Sobrino, J.C. Jiménez-Muñoz, L. Paolini, Land surface temperature retrieval from LANDSAT TM 5, *Remote Sens. Environ.* 90 (4) (2004) 434–440.
- [75] C. Yin, M. Yuan, Y. Lu, Y. Huang, Y. Liu, Effects of urban form on the urban heat island effect based on spatial regression model, *Sci. Total Environ.* 634 (2018) 696–704.
- [76] H. An, H. Cai, X. Xu, et al., Impacts of urban green space on land surface temperature from urban block perspectives, *Rem. Sens.* 14 (2022) 4580.
- [77] M. Hasan, L. Hassan, M.A. Al, et al., Urban green space mediates spatiotemporal variation in land surface temperature: a case study of an urbanized city, Bangladesh, *Environ. Sci. Pollut. Res.* 29 (2022) 36376–36391.
- [78] F. Kong, H. Yin, P. James, L.R. Hutyrá, H. He, Effects of spatial pattern of greenspace on urban cooling in a large metropolitan area of eastern China, *Landsc. Urban Plann.* 128 (2014) 35–47.
- [79] J. Peng, J. Jia, Y. Liu, H. Li, J. Wu, Seasonal contrast of the dominant factors for spatial distribution of land surface temperature in urban areas, *Remote Sens. Environ.* 215 (2018) 255–267.
- [80] W. Zhou, J. Wang, M.L. Cadenasso, Effects of the spatial configuration of trees on urban heat mitigation: a comparative study, *Remote Sens. Environ.* 195 (2017) 1–12.
- [81] J.F. Hair, R.E. Anderson, R.L. Tatham, W.C. Black, *Multivariate Data Analysis*, third ed., Macmillan, New York, 1995.
- [82] A. Buyantuyev, J.G. Wu, Urban heat islands and landscape heterogeneity: linking spatio-temporal variations in surface temperatures to land-cover and socioeconomic patterns, *Landsc. Ecol.* 25 (2010) 17–33.
- [83] X. Dai, Z. Guo, L. Zhang, D. Li, Spatio-temporal exploratory analysis of urban surface temperature field in Shanghai, China, *Stoch. Environ. Res. Risk Assess.* 24 (2) (2010) 247–257.
- [84] H. Li, C.A. Calder, N. Cressie, Beyond Moran's I: testing for spatial dependence based on the spatial autoregressive model, *Geogr. Anal.* 39 (4) (2007) 357–375.
- [85] F. Mumtaz, Y. Tao, G. de Leeuw, et al., Modeling spatio-temporal land transformation and its associated impacts on land surface temperature (LST), *Rem. Sens.* 12 (18) (2020) 2987.
- [86] L. Kong, K.K.-L. Lau, C. Yuan, Y. Chen, Y. Xu, C. Ren, E. Ng, Regulation of outdoor thermal comfort by trees in Hong Kong, *Sustain. Cities Soc.* 31 (2017) 12–25.
- [87] R.A. Spronken-Smith, T.R. Oke, The thermal regime of urban parks in two cities with different summer climates, *Int. J. Rem. Sens.* 19 (11) (1998) 2085–2104.
- [88] E. Jauregui, Influence of a large urban park on temperature and convective precipitation in a tropical city, *Energy Build.* 15 (3–4) (1991) 457–463.
- [89] M.V. Monteiro, K.J. Doick, P. Handley, A. Peace, The impact of greenspace size on the extent of local nocturnal air temperature cooling in London, *Urban For. Urban Green.* 16 (2016) 160–169.
- [90] W. Shih, The cooling effect of green infrastructure on surrounding built environments in a sub-tropical climate: a case study in Taipei metropolis, *Landsc. Res.* 42 (5) (2017) 558–573.
- [91] X. Cao, A. Onishi, J. Chen, H. Imura, Quantifying the cool island intensity of urban parks using ASTER and IKONOS data, *Landsc. Urban Plann.* 96 (4) (2010) 224–231.
- [92] R.T.T. Forman, *Land Mosaics: the Ecology of Landscapes and Regions*, Island Press, 1995.
- [93] S. Sodoudi, H. Zhang, X. Chi, F. Mueller, H. Li, The influence of spatial configuration of green areas on microclimate and thermal comfort, *Urban For. Urban Green.* 34 (2018) 85–96.
- [94] S. Gillner, J. Vogt, A. Tharang, S. Dettmann, A. Roloff, Role of street trees in mitigating effects of heat and drought at highly sealed urban sites, *Landsc. Urban Plann.* 143 (2015) 33–42.
- [95] W. Zhou, G. Huang, M.L. Cadenasso, Does spatial configuration matter? Understanding the effects of land cover pattern on land surface temperature in urban landscapes, *Landsc. Urban Plann.* 102 (1) (2011) 54–63.
- [96] C.C. Vos, P. Berry, P. Opdam, H. Baveco, B.S.J. Nijhof, J. O'Hanley, C. Bell, H. Kuipers, Adapting landscapes to climate change: examples of climate-proof ecosystem networks and priority adaptation zones, *J. Appl. Ecol.* 45 (6) (2008) 1722–1731.
- [97] Y. Jiang, D. Song, T. Shi, X. Han, Adaptive analysis of green space network planning for the cooling effect of residential blocks in summer: a case study in Shanghai, *Sustainability* 10 (2018) 1389.
- [98] L. Shashua-Bar, M.E. Hoffman, Vegetation as a climatic component in the design of an urban street: an empirical model for predicting the cooling effect of urban green areas with trees, *Energy Build.* 31 (2000) 221–235.